UNIVERSITY OF TARTU
Faculty of Science and Technology
Institute of Technology

Oluwaseun E. Fetuga

Transition metal and nitrogen-doped carbon catalysts based on carbide-derived carbon and carbon nanotubes for proton-exchange membrane fuel cell (PEMFC) application

Bachelor's Thesis (12 ECTS)

Curriculum Science and Technology

Supervisor(s):
MSc Jaana Lilloja,
PhD Elo Kibena-Põldsepp
Professor Kaido Tammeveski

Tartu 2022

Transition metal and nitrogen-doped carbon catalysts based on carbide-derived carbon and carbon nanotubes for proton-exchange membrane fuel cell (PEMFC) application

Abstract:

The electrocatalytic oxygen reduction reaction (ORR) activity of transition metals (Fe or CoFe) and nitrogen-doped nanocarbon catalysts was investigated in this work. The carbide-derived carbon and carbon nanotube composite materials were doped with nitrogen and transition metals by pyrolysis. The physical characterisation of the catalysts was carried out by SEM-EDX and BET methods. The ORR activity of the materials was evaluated using the rotating disc electrode method in acidic media. The results showed that the modified ball-milled Fe-N-C material had superior ORR performance in 0.5 M H_2SO_4 solution.

Keywords: Transition metals, Oxygen Reduction Reaction, Doping, Electrocatalysis.

CERCS: Electrochemistry

Siirdemetalli ja lämmastikuga dopeeritud karbiidset pärituolu süsinikul ja süsiniknanotorudel põhinevad katalüsaatormaterjalid prootonvahetusmembraaniga kütuseelemendi (PEMFC) jaoks

Lühikokkuvõte:

Selles bakalaureusetöös uuriti siirdemetallide ja lämmastikuga dopeeritud süsinikmaterjalide elektrokatalüütilist aktiivsust hapniku redutseerimisel. Karbiidset päritolu süsiniku ja süsiniknanotorude komposiitide dopeerimiseks lämmastikuga ning siirdemetallidega, nagu Fe ja Co, kasutati kuumtöötlemist. Katalüsaatorite füüsikaliseks karakteriseerimiseks kasutati SEM-EDX ja BETi meetodeid. Materjalide hapniku redutseerumise aktiivsust hinnati happelises keskkonnas pöörleva ketaselektroodi meetodil. Saadud tulemustest selgus, et BM2-ga modifitseeritud Fe-N-C materjal näitas kõrget hapniku redutseerumise aktiivsust 0,5 M H_2SO_4 lahuses.

Võtmesõnad: Siirdemetallid, hapniku redutseerumisreaktsioon, dopeerimine, elektrokatalüüs.

CERCS: Elektrokeemia

TABLE OF CONTENTS

ABBREVIATIONS

BET	Brunauer-Emmett-Teller
CDC	Carbide-derived carbon
CNT	Carbon nanotubes
CoFe	Cobalt-Iron
EDX	Energy-dispersive X-ray spectroscopy
F-N-C_mix	Iron nitrogen doped CDC/CNT
GC	Glassy carbon
K-L	Koutecky-Levich
ORR	Oxygen reduction reaction
PEMFC	Proton exchange membrane fuel cell
Pt	Platinum
PGM	Platinum Group metals
RDE	Rotating disc electrode
SCE	Saturated calomel electrode
SEM	Scanning electron microscopy

INTRODUCTION

Oxygen reduction reaction (ORR) electrocatalysis, notably in energy storage and conversion devices, is critical to the development of sustainable and clean energy solutions. Fuel cells use air-reducing cathodes to transform chemical energy into electricity. Proton exchange membrane fuel cells (PEMFC) operate under acidic conditions (Shao et al., 2016). To make better ORR catalysts for PEMFCs, we need well-defined activity benchmarks and measurement methods for Pt/C catalysts. This will make sure that the activity of newly proposed catalysts can be compared and evaluated without any confusion (Gasteiger et al., 2005). There are still issues with Platinum group metal (PGM)-based catalysts, such as their high cost, stability considerations and the possibility of CO poisoning, that prevent their widespread use (Lopes et al., 2016) (James et al., 2018) (Li et al., 2017).

Metal-nitrogen-carbon (M-N-C) catalysts for ORR have recently received an enormous amount of attention because of the recent and rapid progress in the field over the past 10 years, including improvements in the electrocatalytic activity, power performance of fuel cells, CO tolerance, and stability and durability, observed in both high and low pH conditions (Zhong et al., 2015) (Brocato et al., 2013) (Elumeeva et al., 2015) (Rojas-Carbonell et al., 2018). Pyrolyzed M-N-C materials and their ORR electrocatalysis at different pH values still need to be better understood to make an ideal choice of such catalysts in terms of operating conditions, particularly concerning the operating pH in a fuel cell device (Sgarbi et al., 2021).

This BSc thesis is an extension of a previous work in which M-N-C catalysts, particularly iron, cobalt and the mixture of these metals (cobalt-iron) and nitrogen doped carbide-derived carbon and carbon nanotubes, was studied in alkaline medium (Lilloja et al., 2021), but now the goal was to investigate the electrocatalytic activity of transition metals such as iron (Fe) or cobalt-iron (CoFe) and nitrogen-doped carbon nanotubes and carbide-derived carbon, towards the ORR in acidic conditions, to design new and better electrocatalysts from these supports and to establish structure-property relationships that would allow for new advancements in fuel cell electrocatalysis.

1 LITERATURE REVIEW

Overusing fossil fuels has caused big problems for the environment, and every day it becomes more important to deal with the effects of climate change. To avoid any further CO_2 emissions into the environment, reliance on non-renewable energy sources such as coal, gas, or oil should be minimized to transition to a zero-emissions method of energy production. Because of this, renewable energy sources are needed. The hydrogen plays an alternative to fossil fuel because it is a sustainable and non-polluting energy carrier that can be used in stationary and mobile power devices including fuel cells (Ratso et al., 2016). A fuel cell is a device that transforms the chemical energy from the fuel (for example H_2) and the oxidant (e.g O_2) directly into electrical energy (Wang et al., 2011). Polymer electrolyte fuel cells (PEFCs), solid oxide fuel cells (SOFCs), alkaline fuel cells (AFCs), molten carbonate fuel cells (MCFCs), and phosphoric acid fuel cells (PAFCs) are all examples of fuel cells that have gotten the most attention in fuel cell research so far (Wang et al., 2011). In terms of transportation PEFCs are better because they work at low temperatures usually less than 100 °C and they do not need substances or components that are harmful, for instance the phosphoric acid among others (Pasupathi et al., 2016). Therefore, they are perfect for use in vehicles not just because they are safe but also for the fact that they are efficient (Ratso et al., 2016).

In general, it is possible to divide PEFCs into three following ones: proton exchange membrane fuel cell (PEMFC), direct menthol fuel cell and lastly anion exchange membrane fuel cell (Li et al., 2021). For example, in case of PEMFC hydrogen is used as a fuel, protons are released from the hydrogen, which is oxidized at the anode. The protons are transported to the cathode through a proton exchange membrane (PEM). As a result, oxygen is reduced to water at the cathode and water is the desired product when this fuel cell operates (Ratso et al., 2016).

1.1 Proton exchange membrane fuel cell

The PEMFC stack is made up of a membrane electrode assembly (MEA) and bipolar plates, which act as current collectors and provide reagents to the MEA electrodes. The MEA is the part of the stack that generates the fuel cell's electricity. Bipolar plates also connect MEAs together electrically in a series (Kraytsberg et al., 2014). Due to their high power density and efficiency, PEM-based fuel cells are among the most promising electrochemical energy

conversion devices (Tellez-Cruz et al., 2021). The responsibility of proton conductivity in the proton exchange membrane fuel cell is for PEM which transports protons from the anode to the cathode, establishing the important component of the electrochemical device as it can be seen in (Figure 1) (Tellez-Cruz et al., 2021).

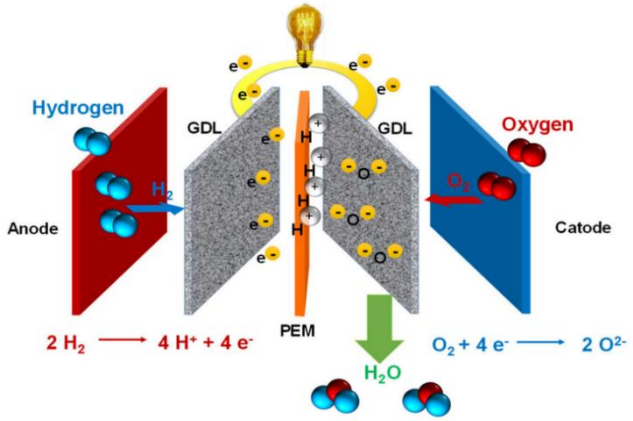

Figure 1. Fuel cell components like anode, cathode, gas diffusion layer and proton exchange membrane are shown in this schematic representation of PEMFC (Tellez-Cruz et al., 2021).

Anode and cathode which function as electrodes must hold a catalyst for the electrochemical reaction to proceed. The optimal catalyst for both the oxygen reduction reaction (ORR) and the hydrogen oxidation reaction (HOR) (Yuan, et al., 2010) are platinum and platinum group metal (PGM)-based electrocatalysts. However, these are high-priced noble metals that are always subject to market volatility. Current PGM cathode catalysts reduce overpotentials for ORR activation and retain adequate stability in an oxidative and acidic environment (Hou, et al., 2020). As a result, the most important objective is to create highly active and stable PGM-free catalysts as low-cost alternatives to PGMs for advanced PEMFCs in order to speed up the development of appealing hydrogen technologies in the future (Wang, et al., 2019).

1.2 Oxygen reduction reaction (ORR)

Oxygen reduction reaction has been an important topic of debate and tireless investigation throughout the previous century (B. Liu and Bard, 2002). ORR plays a great role in energy conversion devices, especially in metal-air batteries and fuel cells, including PEMFCs (Zhang, 2008) (B. Liu and Bard, 2002).

In acidic solutions, the ORR occurs as follows (Anastasijević et al., 1987) (Ross et al., 1998):

The four electrons pathway:

$O_2 + 4H^+ + 4e^- \rightarrow 2H_2O$ $E_0 = 1.229$ V (1)

Or in the case of a two-electron pathway:

$O_2 + 2H^+ + 2e^{--} \rightarrow H_2O_2$ $E_0 = 0.67$ V (2)

Afterwards, hydrogen peroxide is further reduced:

$H_2O_2 + 2H^+ + 2e^{--} \rightarrow 2H_2O$ $E_0 = 1.77$ V (3)

Or it disproportionates:

$2H_2O_2 \rightarrow 2H_2O + O_2$ (4)

The electrocatalyst is often used to introduce the four-electron reduction of O_2 to water (Shao, 2016). Although several catalysts are available for the ORR, the Pt catalyst is usually the most often used. Pt is considered one of the best catalysts in terms of ORR because it can withstand acidic conditions. There is, however, one problem with platinum. It would be difficult to use it in fuel cells considering its rarity and the high cost. Therefore, it has pushed for more research to be conducted to substitute the precious metal catalysts for alternative ones (Sealy, 2008).

1.2.1 Non-precious metal catalysts for the ORR

Among the most promising ways to reduce the cost of PEM fuel cells is to decrease the usage of platinum in the catalyst layers, which has been the most prevalent approach to reduce the cost. This method only works by mixing the Pt with transition metals such as cobalt (Co), iron (Fe). Pt-based catalysts have witnessed a remarkable improvement in mass activity and specific activity, nevertheless this method could not be sustained, because merging these advancement made on the catalyst level to full-size fuel cell stacks has proved to be difficult (Pollet et al., 2019) (Nakamura et al., 2019) (Shao et al., 2016). So, a novel approach is based on synthesising non-precious metal-based electrocatalysts. Reviewing the non-precious metal-based catalysts development for the PEM fuel cell applications, the research has become quite large, covering a wide range of materials. Sadly, the performance of the best non-precious metal catalysts

(usually carbon supported Co-N and Fe-N doped catalysts) is still worse when compared to the performance of Pt-based catalysts in terms of both activity and stability. This has been the case up until today. Despite this, during the past few years, there has been observed an incremental improvement in both the stability and activity of non-precious metal catalysts toward their practical utilization. As a result, these electrocatalysts are now more active and promising. M-N-C materials (where M is Fe, Co, Mn, etc) which are formed by pyrolysis of different metals, carbon and nitrogen precursor materials have been shown to be the most promising so far. Other non-precious metal have been subjected also to research , the non-precious metal include non-pyrolyzed transition metals, metal oxide materials, transition metal chalcogenides among others (Chen et al., 2011) (Pérez-Rodríguez et al., 2021).

1.2.2 Metal nitrogen-doped carbon type catalyst

Electrocatalysis research has recently focused on transition metal and nitrogen-doped carbon (M–N–C) materials as a viable replacement for platinum-based catalysts for the ORR (Y. Zhang et al., 2016). M–N–C electrocatalysts are better in terms of the ORR performance thanks to their efficient active sites, adequate electrocatalytic activity, and durability (Xu et al., 2020).

In contrast, carbon alone does not have a significant impact on the ORR. So far, transition metals and/or nitrogen where M is iron (Fe), cobalt (Co), copper (Cu) and manganese (Mn) have been most successful in creating ORR active sites without platinum (Shao et al., 2016) (Barkholtz and Liu, 2017). It was pointed out that the modification of the structure that normally occurs within the heat-treatment (or pyrolysis), these active materials can be obtained from a lot of chemical precursors such as transition metal salts, sources of carbon and nitrogen (Monteverde Videla et al., 2016).

1.2.3 Active sites for the ORR

To address the issues (high cost, CO_2 poisoning, and scarcity) with ORR catalysts which is the commercial available Pt, a lot of research has been done over the recent decades to come up with active sites (M-N_x, Pyridinic-N) in the catalyst as shown in (Figure 2) that work as well as Pt but are cheaper and more stable (Nakamura et al., 2019).

M-N_x is a metal-based catalytic centre in which the iron atom is coupled to multiple (typically 4) nitrogen atoms. This is one of the most common types of active sites for ORR found in M-

N-C catalysts (Figure 2) (Zitolo et al., 2015) (Jia et al., 2016) (Tellez-Cruz et al., 2021a). M-N_x sites are believed to be responsible for a 4-electron ORR in acidic medium (Zitolo et al., 2015).

Carbon's electrons are conjugated to nitrogen's lone-pair electrons by adding electron-rich nitrogen atoms into the carbon support (Zhao et al, 2013). The impact of nitrogen doping is dependent mainly on the lattice arrangement of the dopant atoms. Pyridinic-N is one of the nitrogen species found in N-doped carbon-based materials (Domínguez et al., 2015) (Q. Liu et al., 2012). There are other nitrogen functional groups which include pyrrolic-N and graphitic-N (Nakamura et al., 2019).

Pyridinic-N atoms have long been assumed to be responsible for the ORR activity because of the π-conjugation carbon network it produces which means that they could be used a base or starting point for platinum substituted catalyst (Nakamura et al., 2019) (Donghui et al., 2016) (Mamtani et al., 2016)

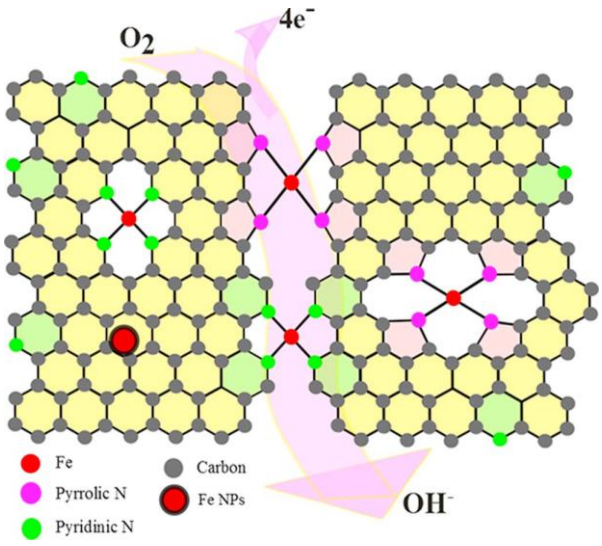

Figure 2. Showing Fe-Nx (Fe) and Pyridinic N in the M-N-C catalysts (Jia et al., 2016).

1.3 Nanocarbons as supporting materials

The features of large specific surface area, electrical conductivity, chemical stability, and porosity are some of the characteristics that are shared by carbon nanomaterials for example carbide-derived carbon (CDC) and carbon nanotubes (CNTs) (Ratso et al., 2016). This contributes to their use as catalyst supports. Electrons needed for O_2 reduction can be transported to these active site (M-N_x and Pyridinic N) thanks to electrical conductivity, because the materials are also chemically inert, the carbon itself is highly durable (even though it can be oxidized when a fuel cell is working) (Ratso et al., 2016). The porous structure contributes

to the mass transport in the catalyst layer and a large surface area is favourable for the creation of a higher number of active sites (Ratso et al., 2018) (Ratso et al., 2016). Carbon nanotubes were a scientific and technological breakthrough. Appropriate engineering of them could lead to the development of novel materials for a range of uses. Due to their open structure and high polarity, carbon nanotubes can improve the properties and performance of other materials (Amin et al., 2020). Carbon nanotubes can exist in both single-walled and multi-walled forms (Figure 3a) (Mtukula et al., 2016). The single-walled CNT consists of a single wrapped graphene sheet with a tubular structure. On the other side, multi-walled CNTs are a mixture and collection of concentric single-walled carbon nanotubes (Amin et al., 2020).

When the metal or semi-metal atoms from the carbide lattice is removed, a porous carbon network is left behind. This is what is known as a carbide-derived carbon (CDC) (Figure 3b). CDCs have the potential to alter the porosity of carbon, allowing for a wide range of pore sizes (large and small) to be achieved. Their large specific surface area and porosity make them ideal for commercial supercapacitors and fuel cells (Lilloja et al., 2021). Changing the temperatures at which the carbide and chlorination reactions begin has a large impact on the surface area, disorder, and pore size distribution (Dash et al., 2005).

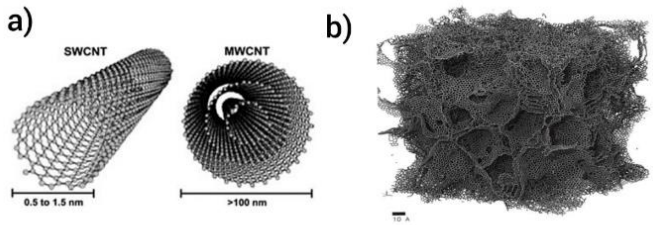

Figure 3. (a) Structures of single-walled CNTs and multi-walled CNTs (Ribeiro et al., 2017) and (b) carbide-derived carbon (Zhan et al., 2017).

Doping of Nano-Carbons

It is possible to dope the carbon material using the process which involves creating a combination of carbon support material, nitrogen, and transition metal dopants (often an inexpensive salt) and pyrolysis. Pyrolyzing the dopants and carbon substrate at high temperature creates active sites in the final catalyst material for the ORR. The precursors are usually combined either in liquids (via sonication) or in solid form (via ball-milling) before being pyrolysed at high temperatures (Vikkisk et al., 2013) (Lefèvre et al., 2009) (Wu et al., 2011).

Sonification

Sonication is one of the methods often used for mixing reagents (e.g. transition metals and nitrogen containing precursors) with existing nanocarbons (e.g. CDCs and CNTs) to disperse the materials. This process involves using ultrasound to stir the catalyst. Low viscosity solutions (involves water, acetone, or ethanol) containing nanocarbons is best dispersed by sonification. Most of the time, this is done with an ultrasonic bath also called a sonicator (Gou et al., 2012). Based on the literature, sonication is even used for removing graphene sheets from graphite. Heating the fluid containing graphite is an option. However, it is not as successful as sonication in producing graphene. The frequency, amplitude, and power of the sonication system will impact the final graphene product. It is possible to use ultrasonic energy in sonication baths or tips to apply it to nanocarbon-containing dispersions (Warner et al., 2013).

Ball milling

Ball milling was initially intended to grind sample materials to minimise particle size. Furthermore, ball milling may be used to activate chemical processes, create nanostructured materials, and change the reactivity of as-milled solids. Ball milling has a minimal cost of installation and operation, making it an economically viable approach. It may be possible to produce functionalized carbons with rich defects by using the ball-milling technique at a low cost and high yield (Wang et al., 2021) (Wang et al., 2020).

Ball milling offers several benefits. Ball milling shown in (Figure 4a), instead of solution-based impregnation approach, places most of the dopants close to the carbon material's surface, making it easier to create the active sites during electrocatalysis (Ratso et al., 2018).

Pyrolysis

Pyrolysis is the thermochemical decomposition of substances at high temperatures in an inert environment (Figure 4b), such as Ar or N_2. It can be used to create carbon materials from biomass and organic precursors as an example, and to restructure pre-existing carbons (Wang et al., 2020).

For the preparation of functionalised carbon materials, the pyrolysis is widely used, due to its simplicity and cost-effectiveness (Wang et al., 2020). The composition, structure, and morphology of the carbon-based material are strongly influenced by pyrolysis conditions such

as the pyrolysis temperature, gas environment, heating rate, and reaction time. Pyrolysis temperature may affect the degree of graphitization and electrical conductivity, but it can also affect clustering and diminish graphitization at the same time. During pyrolysis, it is possible to easily incorporate heteroatom dopants into the carbon framework by merely calcining the carbon precursor in the presence of heteroatom sources. Some examples of heteroatom sources include dicyandiamide, H_2S, and melamine. So, if the temperature of the pyrolysis is too high it can lead to unstable heteroatom dopants and the surface area for the catalyst can be reduced. For this reason, it is necessary to optimize the pyrolysis conditions in order to acquire practical characteristics in the produced substance (Wang et al., 2021) (Wang et al., 2020).

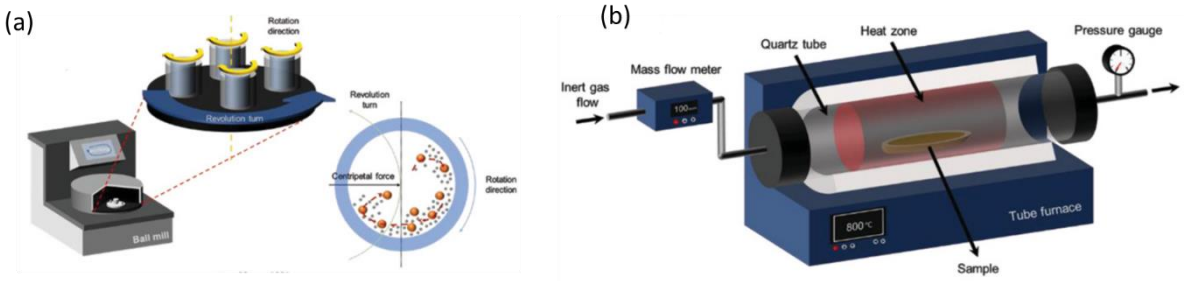

Figure 4. (a) Schematic of ball-milling and (b) schematic of pyrolysis (Wang et al., 2020)

2 THE AIMS OF THE THESIS

The main goals of this research are the following:

- Synthesise transition metal and nitrogen doped CDC/CNT composites
- Study the electrocatalytic activity of these materials towards the ORR in an acidic environment.
- Study the surface and elemental composition of prepared transition metal and nitrogen doped nanocarbons.

3 EXPERIMENTAL PART

3.1 Synthesis of M-N-C catalyst

Carbide-derived carbon (CDC) which was acquired from Skeleton Technologies OÜ (Estonia), was produced by chlorinating silicon carbide. Multiwall carbon nanotubes (NC3150; >95% purity) were purchased from Nanocyl SA (Belgium). As a nitrogen source, 1,10-phenanthroline (purity >99%; Acros Organics) was utilized, while iron(II) acetate (purity 95%; Sigma-Aldrich) and cobalt(II) acetate (purity >98%; Alfa Aesar) were utilized as metal precursors. In all materials, CDC and CNT were taken in equal proportions by weight, the amount of iron(II) acetate corresponded to 1 wt% of Fe relative to the carbon mass and for dual doping (cobalt-iron) 0.5 wt% of Fe and 0.5 wt% of Co were added.

Prior to the preparation of iron and nitrogen doped CDC/CNT (Fe-N-C_mix) and cobalt-iron nitrogen doped CDC/CNT (CoFe-N-C_mix), the CDC material was ball-milled. For the wet-ball milling, 200 mg of CDC material, 20 mg of polyvinylpyrrolidone (PVP, MW = 40000; Sigma-Aldrich), 3 mL of ethanol, and 20 g zirconium dioxide balls (diameter 0.5 mm) were placed in the grinding bowl. The ball milling was done at 400 rpm for 2 h (4 × 30 min, 5 min cooling breaks). An ultrasonic bath was used for 30 min to treat the mixture of metal acetate and 1,10-phenanthroline in the first step of catalyst synthesis. A sonication step was then performed for at least 30 min (Figure 5a) until all the CDC, CNT, and additional PVP had been dispersed evenly. The prepared liquid dispersion was dried overnight in an oven at 60 °C. The obtained powder was then pyrolyzed in an inert atmosphere (N_2, 99.999%, Linde). The sample was inserted into the heating zone at 800 °C, kept there for 1 h, and then quickly removed, after which the obtained catalyst material was collected.

To create Fe-N-C_BM1 material, previously ball-milled CDC, CNTs, PVP, 1,10-phenanthroline, and iron (II) acetate were combined using wet ball-milling at 400 rpm for 1 h (20g ZrO_2 balls with diameter 0.5 mm, 5 ml ethanol). The slurry was dried in an oven at 60°C, then pyrolyzed for 1 h at 800°C.

In order to make Fe-N-C_BM2 material, the original CDC (no ball-milling), CNTs, PVP, 1,10-phenanthroline, and iron (II) acetate were mixed by wet ball-milling at 400 rpm for 2 h (20g ZrO_2 balls with diameter 0.5 mm, 5 ml ethanol). The slurry was dried in an oven at 60°C, then pyrolyzed for 1 h at 800°C.

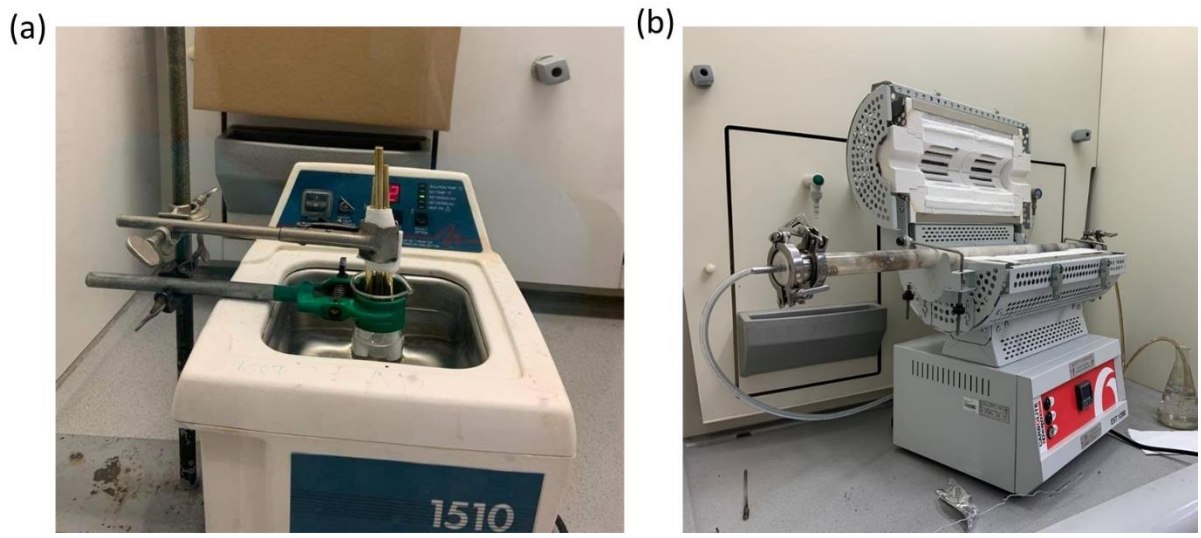

Figure 5. (a) Image of ultrasonic bath used during experiment and (b) pyrolysis oven used during experiment.

Two different acid treatment procedures (designated as AT1 and AT2) were used with Fe-N-C_BM2 material to remove inactive metal species from the catalyst.

The Fe-N-C_BM2_AT1 catalyst was made by adding acid mixture of 0.5 M H_2SO_4 and 0.5 M HNO_3 to the ball milled catalyst (Fe-N-C_BM2). It was then sonicated to mix thoroughly for 10 min. After that, a magnetic steerer with heating was used to stir the catalyst in acid mixture for 8 h at 50 $^{\circ}$C.

Fe-N-C_BM2_AT2: To make this acid treated material, we used an acid solution of 0.5 M H_2SO_4. We also used a magnetic steer as done on previous occasions, but in this case, 80 $^{\circ}$C was used for 8 h during mixing.

Following the acid treatment, the material was washed with deionised water (until neutral pH), filtrated and dried in an oven at 60 °C. After acid treatment, the materials were subjected to the second pyrolysis for 1 h at 800 °C.

3.2 Electrode preparation

The catalyst materials were deposited on glassy carbon (GC) electrodes having a geometric area of 0.196 cm^2. The GC discs (GC-20SS, Tokai Carbon, Japan) were mounted onto Teflon®

holders and polished with 1 and 0.3 μm alumina slurry (Buehler), then sonicated in Milli-Q water and 2-propanol for 5 min in each solvent to remove polishing debris.

For the measurements in 0.5 M H_2SO_4, 5 mg of Fe-N-C was added to a suspension using 490 μL of Milli-Q water, 490 μL of 2-propanol and 20 μL of 5% Nafion® solution. In this case, the suspension was sonicated for 60 min. Once the suspension was made and the electrodes are clean of polishing debris, a specific amount of suspension was drop cast onto the GC electrode, giving a catalyst loading of 0.6 or 0.8 mg cm^{-2}, followed by drying in the oven at 60 ^{o}C.

3.3 Electrochemical measurements

Electrochemical measurements were conducted using the three-electrode system (Figure 6), where GC electrode coated with corresponding catalyst served as the working electrode, Pt wire as a counter electrode, and saturated calomel electrode (SCE) was used as a reference electrode. The three-electrode electrochemical cell filled with 0.5 M H_2SO_4 (purity 96%) solution was used to carry out the experiments at room temperature (23 ± 1 °C). The solution was then saturated for about 30 min with oxygen before the experiment started. Once saturated, measurement of cyclic voltammograms was done at 200 mV/s first to stabilise the electrode before the rotating disk electrode (RDE) measurements.

The RDE experiments were undertaken using five different rotation rates (ω): 360, 610, 960, 1900 and 3100 rpm. The experiments were controlled using an Autolab potentiostat/galvanostat PGSTAT30 (Eco Chemie B.V., The Netherlands) via General Purpose Electrochemical System (GPES) or NOVA 2.0 software.

Figure 6. Picture of the 3-electrode system used for electrochemistry measurements.

The RDE polarization curves for the all catalysts were recorded in 0.5 M H_2SO_4 at various rotation speeds and the data analysis was done using the Koutecky-Levich (K-L) equation:

$$\frac{1}{I} = \frac{1}{I_k} + \frac{1}{I_d} = -\frac{1}{nFAkC_{O_2}^b} - \frac{1}{0.62nFAD_{O_2}^{2/3}\nu^{-1/6}C_{O_2}^b\omega^{1/2}} \quad (5)$$

Where I is the measured current, I_k and I_d are the kinetic and diffusion-limited currents, respectively; k is the electrochemical rate constant for O_2 reduction; A is the geometric area of the electrode (0.196 cm^2); F is the Faraday constant (96,485 C mol^{-1}); v is the kinematic viscosity of the solution and the following values for O_2 solubility ($c^b = 1.13 \times 10^{-6}$ mol cm^{-3}) and diffusion coefficient ($D = 1.8 \times 10^{-5}$ cm^2 s^{-1}) were used for the K-L analysis in 0.5 M H_2SO_4 solution (Mooste et al., 2018) (Gottesfeld et al., 1987).

3.4 Physico-chemical characterisation of catalysts

Scanning electron microscopy (SEM) was used to study the surface morphology of carbon-based electrocatalysts. To make SEM samples, a specific amount of catalyst was mixed into 2 mL of 2-propanol. Drop casting was used to transfer the suspension on the GC discs. For SEM

experiments, an energy-dispersive X-ray (EDX) spectrometer analyzer INCA Energy 350 (Oxford Instruments) was used with a high-resolution scanning electron microscope (HR-SEM) Helios NanoLab 600 (FEI Company). EDX spectroscopy was used to find out what elements were in catalyst materials and where they were located.

With a NovaTouch LX2 Analyser (Quantachrome) or a Micro-metrics TRISTAR Analyser, the N_2 adsorption/desorption isotherms of the catalyst samples were measured at the boiling point of nitrogen (77 K). Before the N_2 physisorption measurement, the samples were degassed under a vacuum at 200 °C for at least 24 h and then filled with N_2 gas. The Brunauer-Emmett-Teller (BET) theory was used to figure out the specific surface area (S_{BET}) up to a relative N_2 pressure of $P/P_0 = 0.2$. Near the saturation pressure of N_2 ($P/P_0 = 0.97$), the total volume of pores (V_{tot}) was measured. The t-plot method and deBoer statistical thickness were used to figure out the microporosity (V_μ).

It should be noted that the following researchers performed physical characterisation experiments: Dr. Jekaterina Kozlova: SEM-EDX analysis, Dr. Maike Käärik: BET with PSD analysis. However, the author of this bachelor's thesis described the physical characterisation data and conducted the electrochemical tests with corresponding analysis.

4 RESULTS AND DISCUSSION

Results would be the explaining electrocatalytic activity of transition metals and nitrogen-doped carbon nanomaterials towards the oxygen reduction reaction (ORR) in an acidic environment and physico-chemical characterization of prepared electrocatalysts.

Comparison of transition metal additives

Two materials were tested in acidic environment by RDE method. First is the iron-nitrogen co-doped CDC/CNT (Fe-N-C_mix) and second is the cobalt-iron nitrogen doped CDC/CNT (CoFe-N-C_mix). They were tested for their ORR activity, to assess a possible substitution for Pt on the cathode of PEMFCs.

The transition metal doped material's comparison began with the effects of Fe-N-C_mix and CoFe-N-C_mix (Figure 7), and it was discovered that the Fe-N-C_mix and CoFe-N-C_mix were less alike based on gotten ORR onset potentials (E_{onset}, the potential at which current density equals to -0.1 mA cm^{-2}) and half-wave potential ($E_{1/2}$, a potential where the current equals to ½ of the diffusion-limited current). The onset potentials of Fe-N-C_mix and CoFe-N-C_mix were 0.60 and 0.53 V, respectively, while the half-wave potentials were 0.44 and 0.4 V, respectively.

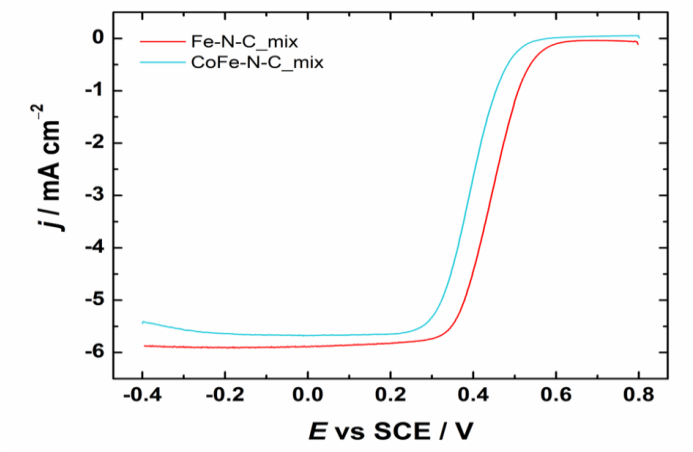

Figure 7. RDE polarisation curves for O_2 reduction of Fe-N-C_mix and CoFe-N-C_mix in O_2-saturated 0.5 M H_2SO_4. v = 10 mV s^{-1}, ω = 1900 rpm, catalyst loading = 0.6 mg cm^{-2}.

Next, the number of electrons transferred per O_2 molecule (n) and the K-L results are compared (Figure 8). According to the K–L plots, when the overpotential is high, parallel K–L lines yield intercepts bypassing the origin of the axis, which indicates that the electroreduction of oxygen is limited by mass transfer to the electrode surface. The value of n was determined by

calculating from the slopes of the K-L plots. Observation indicates that the number of electrons was four in the case of Fe-N-C_mix, still, for CoFe-N-C_mix, the *n* value was around 3.8 which means that O_2 might not have been completely reduced and peroxide might have been produced, and hydrogen peroxide is an unwanted substance for fuel cells (Lee et al., 2021). In the case of Fe-N-C_mix, interpreting the K-L plot to the y-axis yields an intercept around zero, indicating that the ORR process was completely controlled by diffusion.

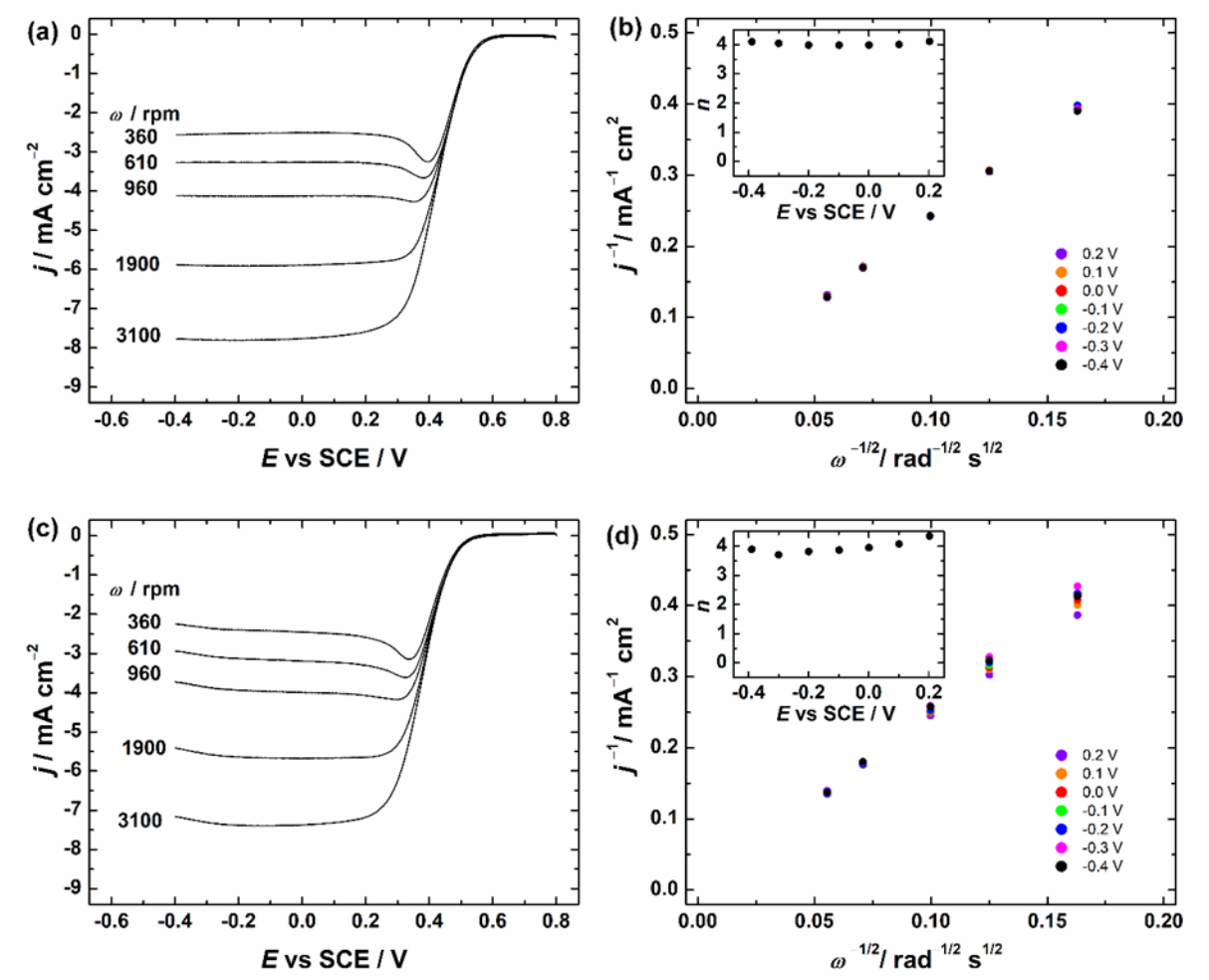

Figure 8. (a, c) RDE voltammetry curves for oxygen reduction in O_2-saturated 0.5 M H_2SO_4 with varying rotation rates; (b, d) K-L plots and the number of electrons transferred per O_2 molecule as a function of potential for (a, b) Fe-N-C_mix (c, d) CoFe-N-C_mix catalysts.

According to the literature, solely nitrogen-doped catalysts are ineffective in acidic environments; however, transition metal-based catalytic systems are an effective alternative (Ratso et al., 2016). Previous research has shown that Fe-containing catalysts are more active for ORR than their Co-containing conterparts in acidic conditions (Kuznetsov, 2009).

For the reasons which include higher half-wave potential, and that the ORR follows a 4-electron pathway, we decided to choose the iron as the metal additive to further investigate by preparing two Fe-N-C catalysts by ball-milling. Thus, the following work was carried out with Fe-N-C catalyst because it was more active than CoFe-N-C catalyst towards the ORR.

Comparison of various synthesis of Fe-N-C_mix catalyst

The ORR investigations in the acidic medium were conducted on Fe-N-C_mix, as well as on Fe modified ball-milled materials (Fe-N-C_BM1 and Fe-N-C_BM2). The effect of two different ball-milling incorporated mixing techniques in an acidic environment was studied using the RDE method. The K-L analysis was carried out to see the influence on the *n* value. This comparison was done to check for effect of the modified synthesis (ball-milling) on the materials, if it would yield a higher $E_{1/2}$ and give better results in terms of ORR activity. Both catalysts (Fe-N-C_BM1 and Fe-N-C_BM2 shown in (Figure 9) had similar results towards the ORR in an acidic medium where Fe-N-C_BM1 had the $E_{1/2}$ value of 0.46 V and Fe-N-C_BM2 had the $E_{1/2}$ value of 0.45 V, and their E_{onset} was 0.6 V, which was a positive result compared to the Fe-N-C_mix material which had 0.44 V as $E_{1/2}$.

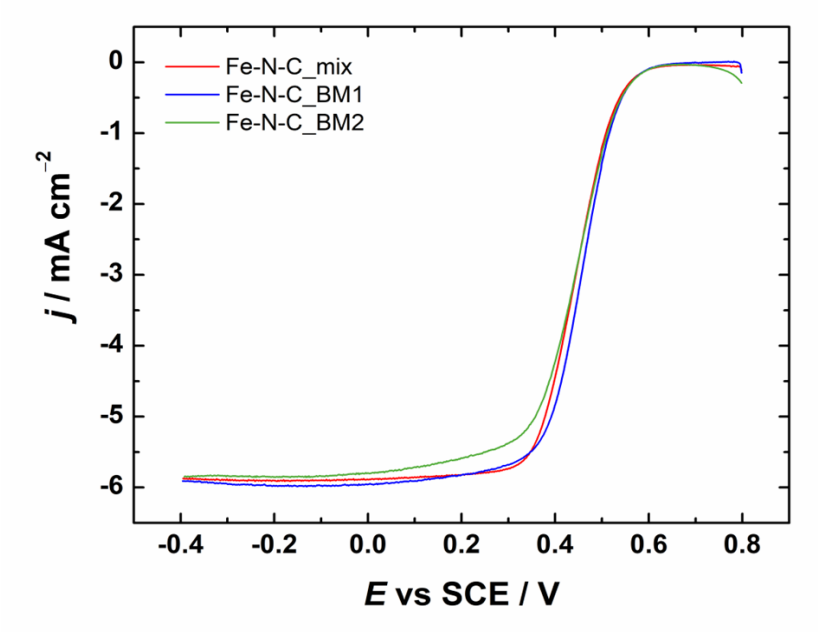

Figure 9. RDE polarisation curves for O_2 reduction on Fe-N-C_mix, Fe-N-C_BM1 and Fe-N-C_BM2 catalysts in O_2-saturated 0.5 M H_2SO_4. v = 10 mV s^{-1}, ω = 1900 rpm, catalyst loading = 0.6 mg cm^{-2}.

A similar K-L study was done for these catalysts (Figure 10), where the K-L plot to the y-axis yields an intercept around zero, which indicates complete diffusion control, and the *n* values are close to 4 in both cases. For both catalysts, at all the potentials that were investigated, the O_2 reduction process most frequently takes place along a four-electron pathway, and the product of the ORR is H_2O.

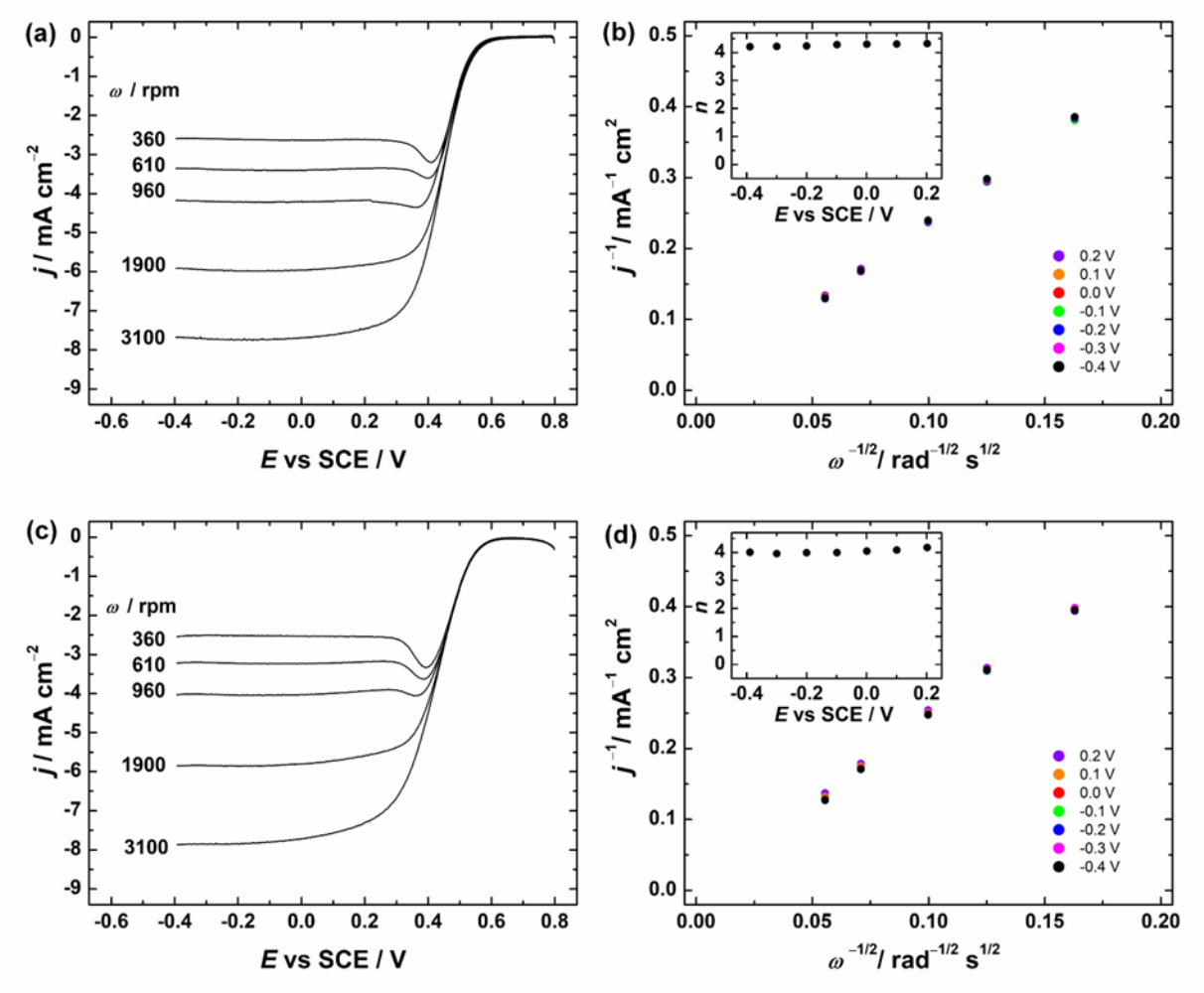

Figure 10: (a, c) RDE polarisation curves for oxygen reduction in O_2-saturated 0.5 M H_2SO_4 at different rotation rates using a scan rate of 10 mVs^{-1}; (b, d) K-L plots and the number of electrons transferred per O_2 molecule for (a, b) Fe-N-C_BM1 (c, d) Fe-N-C_BM2.

The morphology of the materials was studied with obtained SEM micrographs presented in Figure 11. Large-scale micrographs (5µm) show the homogeneous distribution of CDC grains, which are in different sizes. The CNTs have connected all the microporous CDC grains into a network, which has resulted in the material having also both meso- and macropores. This network might be useful in terms of mass transport in the catalyst layer of an PEMFC, primarily at high current densities. Also, the CDC particles are covered by CNTs and the CNTs

themselves are positioned in a variety of ways, with some of them bundled or curled up as shown on the smaller scale (500 nm). The surface looked quite similar compared to the Fe-N-C and CoFe-N-C catalyst shown in previous studies (Lilloja et al., 2020).

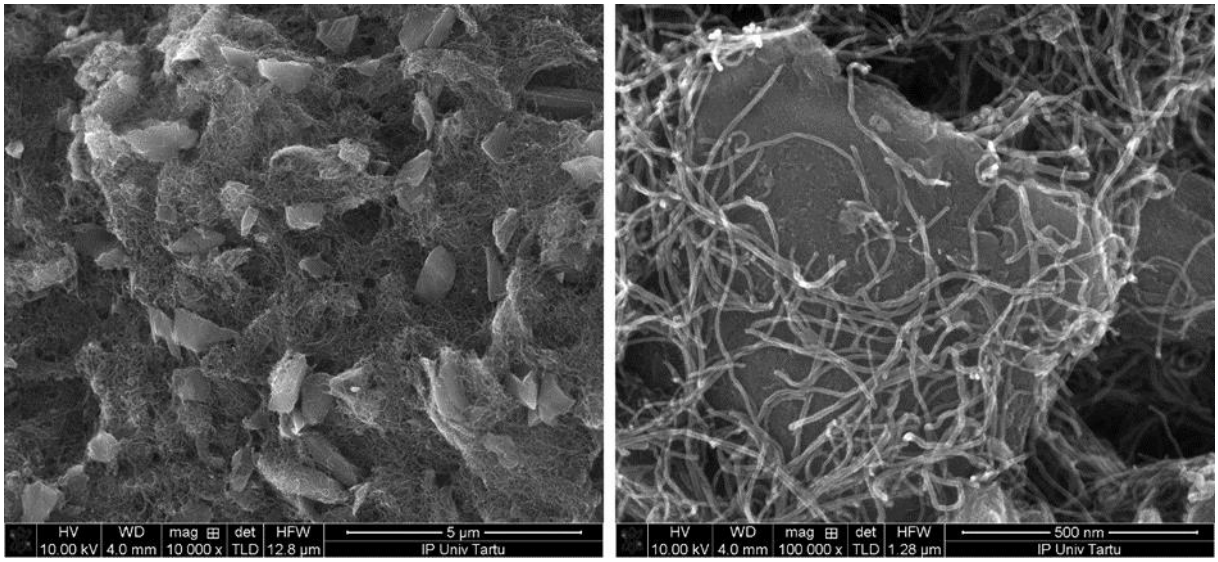

Figure 11. SEM micrographs for Fe-N-C_BM2 sample.

The transition metal and nitrogen doped nano-carbon catalyst were studied using N_2 adsorption. Lowest specific surface area (SSA) of 404 m^2/g, total pore volume (0.58 cm^3g^{-1}) and micropore volume (0.11 $cm^3\ g^{-1}$) were obtained from Fe-N-C_mix material (Table 1). Both Fe-N-C_BM1 and Fe-N-C_BM2 materials had SSA of 484 m^2g^{-1} and 463 m^2g^{-1} respectively, with their micropore volume being of 0.15 $cm^3\ g^{-1}$ and 0.14 $cm^3\ g^{-1}$ respectively, meaning they are a bit different from the Fe-N-C_mix material. This indicates that ball-milling precursors together seems to work better than sonication as slightly higher SSA was achieved and less pores were blocked during doping (higher V_{tot} for Fe-N-C_BM1 (0.71 cm^3g^{-1}) and Fe-N-C_BM2 (0.75 cm^3g^{-1})). It should be noted that the values for Fe-N-C_mix material was obtained from the previous work (Lilloja et al., 2021).

Table 1. Textural properties of metal-N doped CDC/CNT material: pore volume (V_{tot}), micropore volume (V_μ) and specific surface area S_{DFT}.

Catalyst	V_μ, $cm^3\ g^{-1}$	V_{tot}, $cm^3\ g^{-1}$	S_{DFT} $m^2\ g^{-1}$
Fe-N-C_mix	0.11	0.58	404
Fe-N-C_BM1	0.15	0.71	484
Fe-N-C_BM2	0.14	0.75	463

Regarding the pore size distribution (Li et al., 2016) (Shui et al., 2015) claim that micropores, mesopores, or a combination of both are required for efficient Fe-N-C electrocatalysts. It would be of particular interest to investigate the effect of PSD (Figure 12) on Fe-N-C electrocatalytic activity. With the three materials having a micropores less than 2 nm, small mesopores in the range of 3.5 nm as well as larger mesopores (15-20 nm), we can definitely say ball milling has help the materials making it porous. To further give estimation of the porosity, the smaller fraction of V_{tot} was comprised of micropores (V_{μ}) in the case of Fe-N-C_BM1 and Fe-N-C_BM2 than in Fe-N-C_mix.

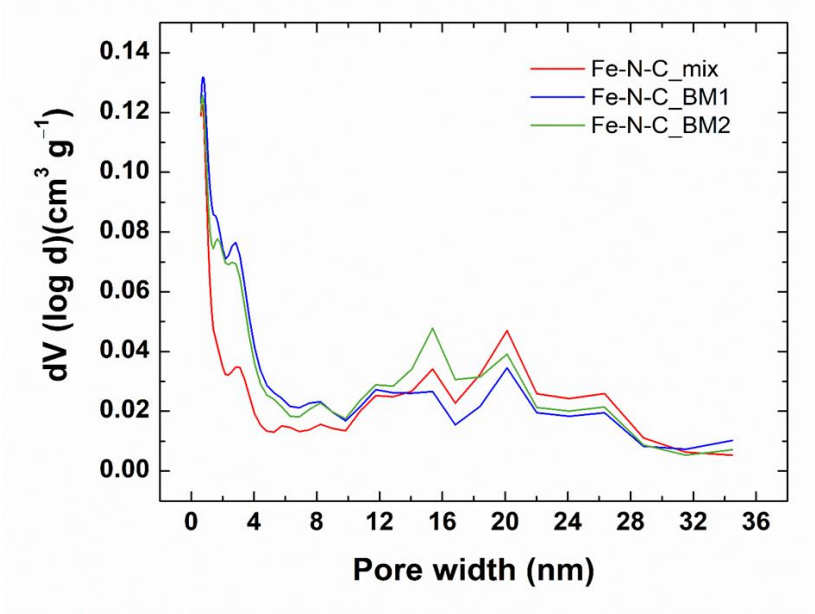

Figure 12. Pore size distribution graphs for Fe-N-C_mix, Fe-N-C_BM1 and Fe-N-C_BM2.

While both Fe-N-C_BM1 and Fe-N-N_BM2 had similar ORR activity and textural characteristics, next step of the work was carried out using Fe-N-C_BM2 because it has less steps in the synthesis process, thus making it easier to produce.

Comparison of acid treated methods

Next, we intended to find out if acid treatment of the catalyst would increase the ORR performance (including the half-wave potential) of the catalyst in the sense that treating with acid might help to remove inactive Fe species from the catalyst. Two different acid treatment procedures were tested and compared on Fe-N-C_BM2 material, the exact procedures are explained in the experimental part. The comparison of the two acid-leached catalysts, Fe-N-

C_BM2_AT1 and Fe-N-C_BM2_AT2, is shown in Figure 13. When the acid-leached catalyst was compared to the original modified ball-milled catalyst for oxygen reduction reaction in an acidic environment, it was observed that ORR electrocatalytic activity of Fe-N-C_BM2_AT1 got worse (half-wave potential of 0.34 V) compared to the other acid-leached Fe-N-C_BM2_AT2 with the $E_{1/2}$ value of 0.45 V with their onset potential of 0.56 and 0.60 V ,respectively.

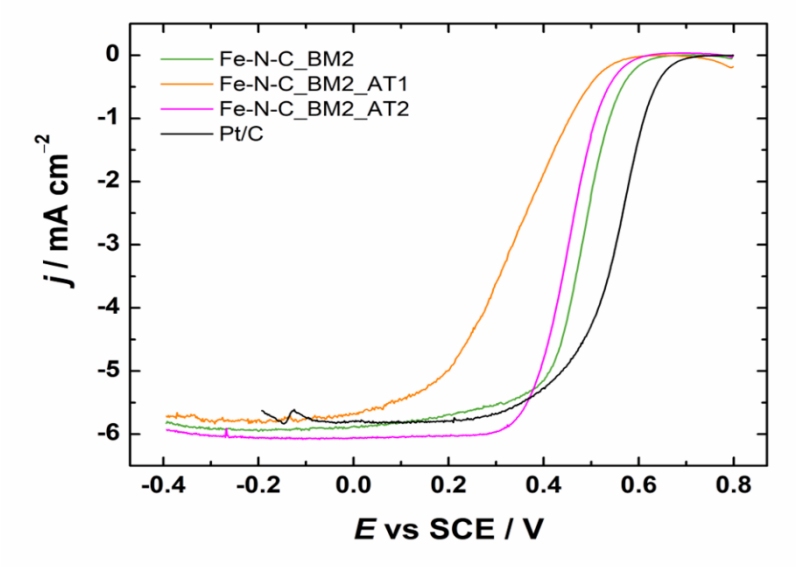

Figure 13. Comparison RDE polarisation curves of Fe-N-C_BM2 vs Fe-N-C_BM2_AT1, Fe-N-C_BM2_AT2 (catalyst loading of 0.8 mg cm^{-2}) and commercial Pt/C catalyst (with loading of 0.02 mg Pt/cm^2) in O_2-saturated 0.5 M H_2SO_4. v = 10 mV s^{-1}, ω = 1900 rpm.

Besides that, the K-L analysis were also conducted for the materials, (Figure 14), where the values of *n* derived from the slopes of the K-L plots can be seen in the insets. Inferring the *n* value reveals that the Fe-N-C_BM2_AT1 is less than 4, which means that oxygen is not fully reduced, and hydrogen peroxide might have been produced, on the other hand, Fe-N-C_BM2_AT2's *n* values were all close to 4 indicating that O_2 has been completely reduced to water, which was the intent.

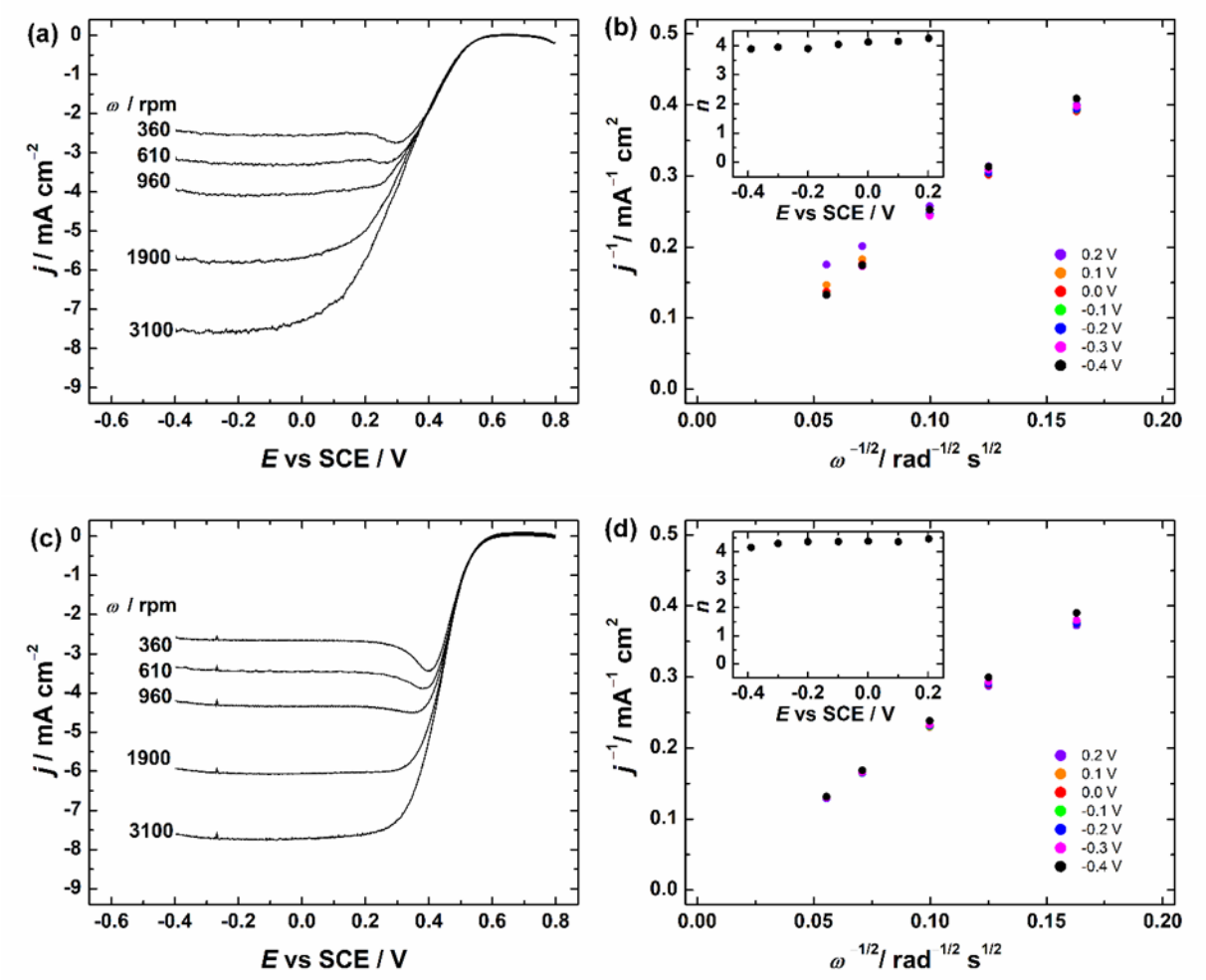

Figure 14: RDE polarisation curves for ORR on (a) Fe-N-C_BM2_AT1 and (c) Fe-N-C_BM2_AT2 modified GC electrodes in O_2-saturated 0.5 M H_2SO_4. ν = 10 mV s^{-1}, K-L plots for O_2 reduction on (b) Fe-N-C_BM2_AT1 and (d) Fe-N-C_BM2_AT2 catalysts in 0.5 M H_2SO_4. Insets show the potential dependence of *n*.

SEM images for Fe-N-C_BM2_AT1 and Fe-N-C_BM2_AT2 (Figure 15 and 16) were used to study the effect of acid treatment on the morphology of materials, however, it is observed that there is no significant change in the structure of both acid-treated materials compared to the untreated material. Their physical appearance appears to be similar when comparing to the Fe-N-C_BM2 sample (Figure 11).

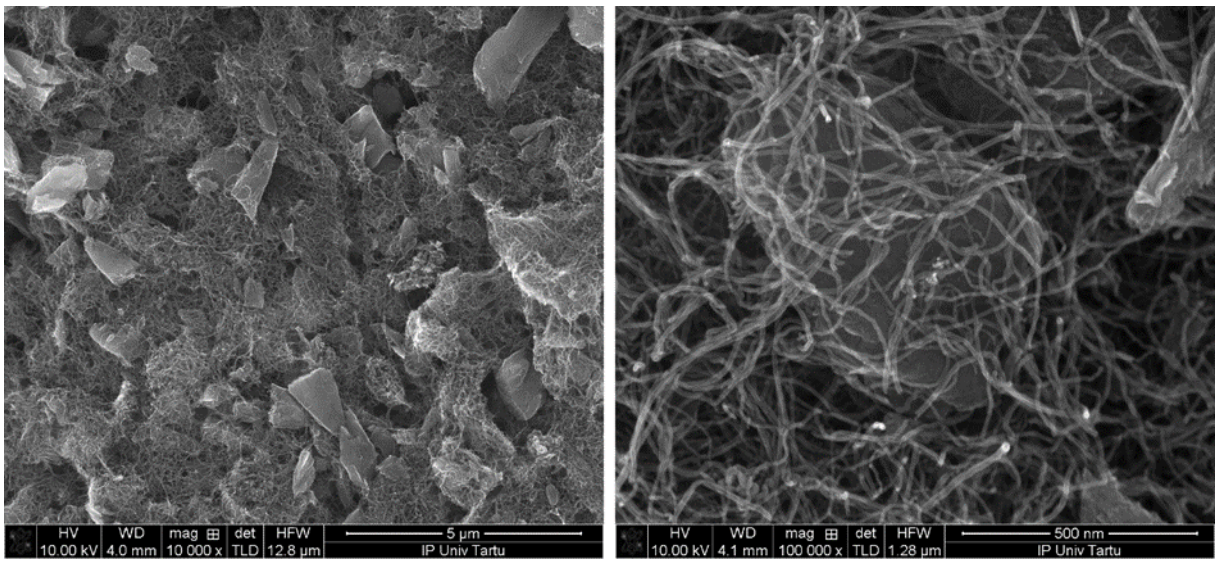

Figure 15. SEM micrographs for Fe-N-C_BM2_AT1 at 10,000x and 100,00x magnification (scale bar: 5 µm and 500 nm).

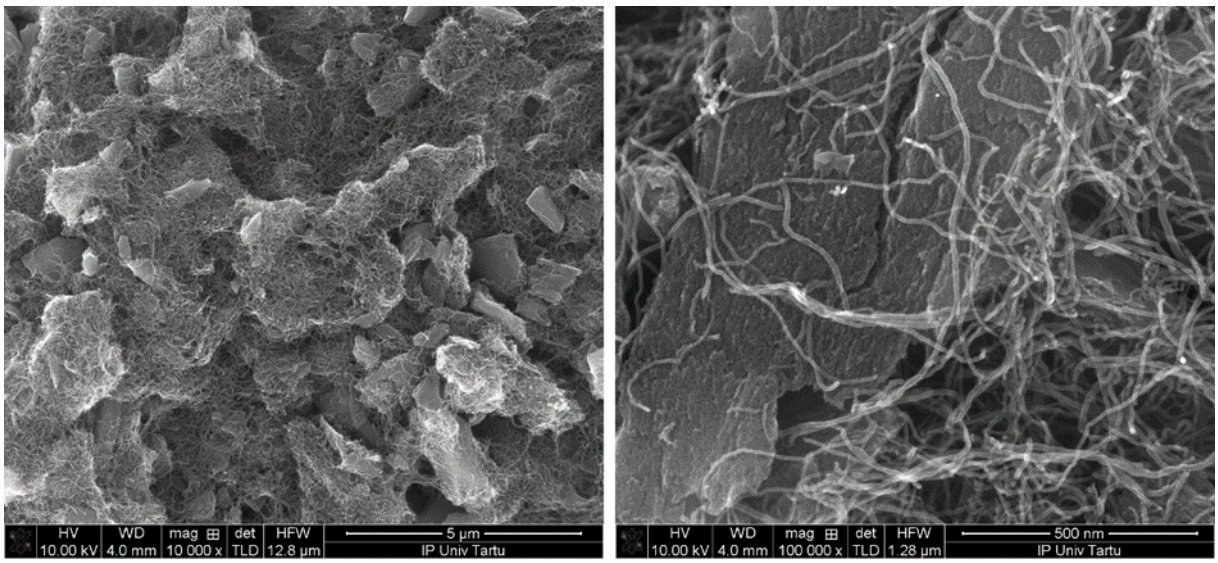

Figure 16. SEM micrographs for Fe-N-C_BM2_AT2 at 10,000x and 100,00x magnification (scale bar: 5 µm and 500 nm).

SEM-EDX method is used to provide information on elemental identification as well as quantitative composition (Ellingham et al.,2017). According to SEM-EDX analysis (Table 2) the Fe-N-C_BM2 catalyst contained 1.15 wt.% of Fe and the acid-leached materials Fe-N-C_BM2_AT1 and Fe-N-C_BM2_AT2 contained 0.88 wt.% and 0.85 wt.% respectively. This suggests that the reduced Fe content in the acid-treated materials was due to the leaching of inactive Fe species, and hence was successful especially in the case of Fe-N-C_BM2_AT2, which had a good ORR activity, but in the case of Fe-N-C_BM2_AT1 we might suggest that some active species have also been removed, therefore loss in ORR activity or maybe the mixed

acid treatment has oxidized the iron in Fe-N-C_BM2_AT1 catalyst material, thus making some sensitive sites.

In addition, we wanted to observe the nitrogen content of the catalyst materials, for Fe-N-C_BM2 (4.54 wt%), for Fe-N-C_BM2_AT1 (4.39 wt%), for Fe-N-C_BM2_AT1 (3.66 wt%), which infers that doping has been successful.

Table 2. Elemental composition (wt%) of Fe-N-C_BM2, Fe-N-C_BM2_AT1 and Fe-N-C_BM2_AT2 materials.

Catalyst materials	C	N	O	Na	Si	S	Fe
Fe-N-C_BM2	90.42	4.54	3.25	0.07	0.34	0.24	1.15
Fe-N-C_BM2_AT1	91.04	4.39	2.94	0.02	0.31	0.43	0.88
Fe-N-C_BM2_AT2	92.54	3.66	2.34	0.02	0.34	0.28	0.85

So far Fe-N-C_BM2 and Fe-N-C_BM2_AT2 are the best performing materials towards the ORR with the Fe-N-C_BM2_AT2 having specific surface area of 480 m^2 $g^{-1,}$ micropores volume of 0.15 cm^3 g^{-1} and total pore volume of 0.69 cm^3 g^{-1} which is almost the same as the Fe-N-C_BM2 having a SSA of 484 m^2 g^{-1}, the micropores volume of 0.14 cm^3 g^{-1} and total pore volume 0.75 cm^3g^{-1}. These similarities can also be seen on the pore size distribution graph against the Fe-N-C_BM2 material (Figure 17). Inferring that acid treatment of Fe-N-C_BM2_AT2 material has not changed the porous structure of the material.

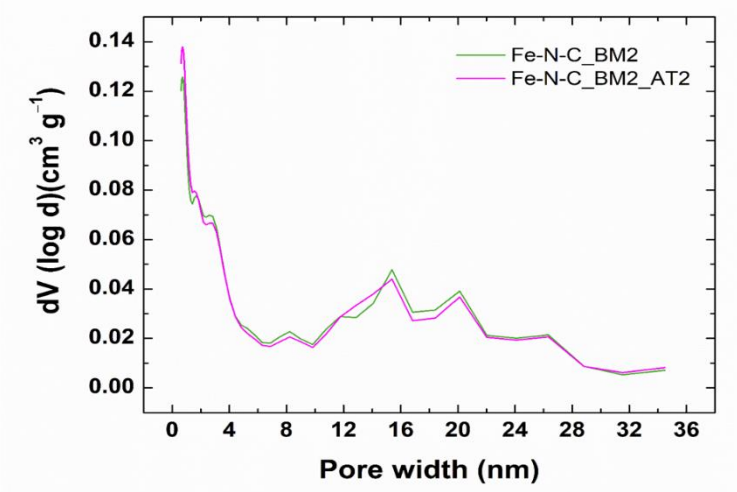

Figure 17. Pores size distribution graph for Fe-N-C_BM2 and Fe-N-C_BM2_AT2

In addition to being active towards ORR the catalyst materials need to be stable to be considered for PEMFC application, which is why Fe-N-C_BM2 and Fe-N-C_BM2_AT2 catalysts were subjected to short-term stability tests (Figure 18). A comparison of the RDE polarisation curves

recorded before and after 10,000 potential cycles (between 0.8 to 0.4 V at 100 mV s^{-1}) in O_2-saturated 0.5 M H_2SO_4 solution shows a decrease in the ORR activity for Fe-N-C_BM2 as the half-wave potential decreased by 40 mV and for Fe-N-C_BM2_AT2 was decreased by 58 mV. Previous studies claimed that the lack of stability of Fe-containing N-doped catalysts in acidic conditions is one of the most significant drawbacks of non-precious metal catalysts for ORR and PEMFC application. This can be caused by a number of factors, including the leaching of the active metal site and oxidation by H_2O_2.(S. Zhang et al., 2013) (Banham et al., 2013)

In this case, leaching of the active metal site is probably not the issue because acid treated material was done to remove sensitive metal species, so stability could be achieved, second reason is the oxidation by hydrogen peroxide, which might be the case herein and based on the literature, when hydrogen peroxide is produced, it reduces the stability of the catalyst material. These result was in accordance with Fe-NCNT-2 material in previous studies (Ratso et al., 2018).

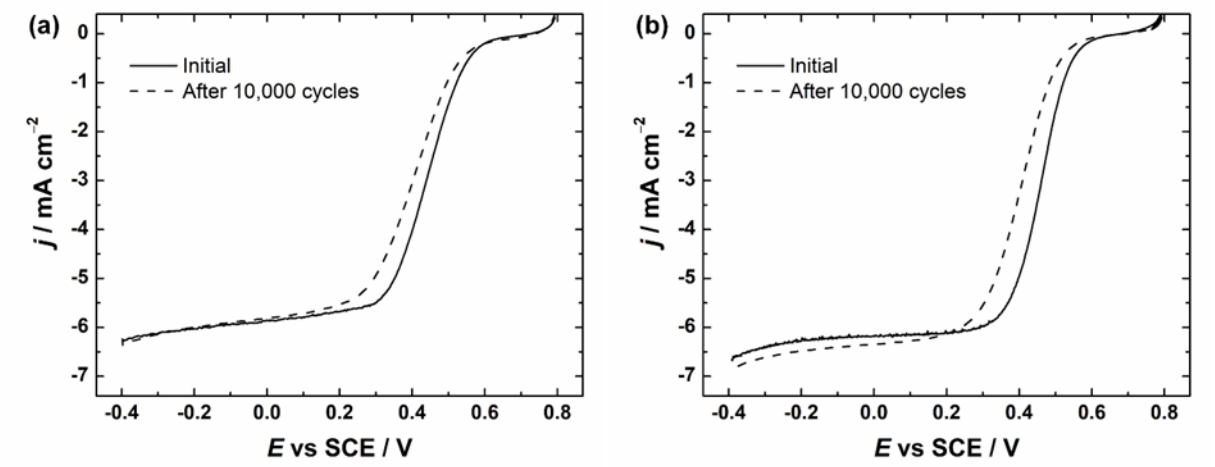

Figure 18. ORR polarisation curves for (a) Fe-N-C_BM2 and (b) Fe-N-C_BM2_AT2 catalyst in 0.5 M H_2SO_4 before and after 10,000 potential cycles. v = 10 mV s^{-1}, ω = 1900 rpm.

Although the Fe-N-C materials had good performance in terms of ORR, the activity of the materials compared to the commercial Pt/C catalyst (Figure 13) have not gotten to the intended point yet. This together with losses in activity during stability test indicate that more research needs to be done to close the gap.

SUMMARY

The objective of this BSc thesis was to investigate the oxygen reduction reaction activity of transition metal and nitrogen doped nanocarbon composites (CDC and CNTs). The doping of all M-N-CDC/CNT catalyst materials was done using a simple high-temperature pyrolysis method for all materials which include CoFe-N-C_mix, Fe-N-C_mix, Fe-N-C_BM1, Fe-N-C_BM2, Fe-N-C_BM2_AT1 and Fe-N-C_BM2_AT2. The sonicated (CoFe-N-C_mix and Fe-N-C_mix), mixed via ball-milling (Fe-N-C_BM1 and Fe-N-C_BM2), and acid treatment (Fe-N-C_BM2_AT1 and Fe-N-C_BM2_AT2) synthesis were made. The success of doping the materials containing N and Fe was assessed using SEM-EDX method. BET results show that feasible porous structure was obtained in all materials. The surface morphology was evaluated using SEM micrographs.

Oxygen reduction reaction studies in 0.5 H_2SO_4 solution utilising the RDE technique shows that Fe-N-C_mix had a better ORR performance than CoFe-N-C_mix giving a half-wave potential of 0.44 V. Furthermore, the studies for ball-milled catalyst (Fe-N-C_BM1 and Fe-N-C_BM2) against the sonicated Fe-N-C_mix, which showed no effect on the ORR activity in RDE measurements, but ball-milling had other benefits (slightly higher specific surface area). Next we compared the acid treatment methods (Fe-N-C_BM2_AT1 and Fe-N-C_BM2_AT2), herein Fe-N-C_BM2_AT2 material, where only 0.5 M H_2SO_4 was used for the acid treatment, had better ORR performance than Fe-N-C_BM2_AT1 (mix of two acids used). Next, the best performing catalysts in this work (Fe-N-C_BM2 and Fe-N-C_BM2_AT2) were subjected to a stability test and results show the half-wave potential decreased by 40 mV and 58 mV, respectively.

To summarize, in the light of the findings gotten from electrochemical characteristics and the physico-chemical characteristics, the results have proven to be of contribution to the field of PEMFC application.

REFERENCES

List of references is presented in alphabetical order.

Amin, R., Kumar, P. R., & Belharouak, I. (2020). *Carbon Nanotubes: Applications to Energy Storage Devices* in *Carbon Nanotubes—Redefining the World of Electronics*. pp. 1–2. https://doi.org/10.5772/intechopen.94155

Anastasijević, N. A., Vesović, V., & Adžić, R. R. (1987). *Determination of the kinetic parameters of the oxygen reduction reaction using the rotating ring-disk electrode: Part I. Theory., Journal of Electroanalytical Chemistry and Interfacial Electrochemistry*, *229*(1), pp. 305–316. https://doi.org/10.1016/0022-0728(87)85148-3

Banham, D., Ye, S., Pei, K., Ozaki, J.I., Kishimoto, T., Imashiro, Y. (2015). *A review of the stability and durability of non-precious metal catalysts for the oxygen reduction reaction in proton exchange membrane fuel cells*. J. Power Sources, vol. 285, pp. 334–348. https://doi.org/10.1016/j.jpowsour.2015.03.047

Barkholtz, H. M., & Liu, D.-J. (2017). *Advancements in rationally designed PGM-free fuel cell catalysts derived from metal–organic frameworks*. *Materials Horizons*, vol. *4*, no. 1, pp. 20–37. https://doi.org/10.1039/C6MH00344C

Bashyam, R., & Zelenay, P. (2006). *A class of non-precious metal composite catalysts for fuel cells*. *Nature*, vol. *443*, no.7107, pp. 63–66. https://doi.org/10.1038/nature05118

Brocato, S., Serov, A., & Atanassov, P. (2013). *PH dependence of catalytic activity for ORR of the non-PGM catalyst derived from heat-treated Fe-phenanthroline*. *Electrochimica Acta*, vol. 87, pp. 361–365. https://doi.org/10.1016/j.electacta.2012.09.053

Chen, Z., Higgins, D., Yu, A., Zhang, L., Zhang, J. (2011). A review on non-precious metal electrocatalysts for PEMfuelcells. Energy & Environmental Science. vol. 4, no. 9, pp. 3167-3192. https://doi.org/10.1039/C0EE00558D

Dash, Yushin, Gogotsi. (2005). *Synthesis, structure and porosity analysis of microporous and mesoporous carbon derived from zirconium carbide*. Microporous and Mesoporous materials. vol. 86, no. 1-3, pp. 50-57. https://www.sciencedirect.com/science/article/pii/S1387181105002416?via%3Dihub

Domínguez, C., Pérez-Alonso, F. J., Abdel Salam, M., Al-Thabaiti, S. A., Obaid, A. Y., Alshehri, A. A., Gómez de la Fuente, J. L., Fierro, J. L. G., & Rojas, S. (2015). *On the relationship between N content, textural properties and catalytic performance for the oxygen*

reduction reaction of N/CNT. *Applied Catalysis B:* vol. 162, pp. 420–429. https://doi.org/10.1016/j.apcatb.2014.07.002

Donghui, G., Shibuya, R., Akiba, C., Saji, S., Kondo, T., Nakamura, J. (2016). *Active sites of nitrogen-doped carbon materials for oxygen reduction reaction clarified using model catalysts*. Science. vol. 351, no. 6271, pp. 361–365. https://www.science.org/doi/10.1126/science.aad0832

Ellingham, S., Thompson, T.J.U., Islam, M. (2017). *Scanning Electron Microscopy-Energy-Dispersive X-Ray (SEM/EDX): A Rapid Diagnostic Tool to Aid the Identification of Burnt Bone and Contested Cremains.* vol. 63, no. 2, pp. 504-510. https://doi.org/10.1111/1556-4029.13541

Elumeeva, K., Ren, J., Antonietti, M., & Fellinger, T.-P. (2015). *High Surface Iron/Cobalt-Containing Nitrogen-Doped Carbon Aerogels as Non-Precious Advanced Electrocatalysts for Oxygen Reduction*. *ChemElectroChem*, vol. 2, no. 4, pp. 584–591. https://doi.org/10.1002/celc.201402364

Gasteiger, H. A., Kocha, S. S., Sompalli, B., & Wagner, F. T. (2005). *Activity benchmarks and requirements for Pt, Pt-alloy, and non-Pt oxygen reduction catalysts for PEMFCs*. *Applied Catalysis B: Environmental*, vol. 56, no. 1, pp. 9–35. https://doi.org/10.1016/j.apcatb.2004.06.021

Gottesfeld, S., Raistrick, I. D., & Srinivasan, S. (1987). *Oxygen Reduction Kinetics on a Platinum RDE Coated with a Recast Nafion Film*. *Journal of The Electrochemical Society*, vol. 134, no. 6, pp. 1455. https://doi.org/10.1149/1.2100689

Gou, J., Zhuge, J., & Liang, F. (2012). Processing of polymer nanocomposites. In S. G. Advani & K.-T. Hsiao (Eds.), *Manufacturing Techniques for Polymer Matrix Composites (PMCs)*. Vol. 4 pp. 95–119. https://doi.org/10.1533/9780857096258.1.95

Hou, J., Yang, M., Ke, C., Wei, G., Priest, C., Qiao, C., Wu, G., Zhang, G. (2020). *Platinum-group-metal catalysts for proton exchange membrane fuel cells: From catalyst design to electrode structure optimization. EnergyChem.* vol. 2, no. 1, pp. 1. https://doi.org/10.1016/j.enchem.2019.100023

Jia, Q., Ramaswamy, N., Tylus, U., Strickland, K., Li, J., Serov, A., Artyushkova, K., Atanassov, P., Anibal, J., Gumeci, C., Barton, S. C., Sougrati, M.-T., Jaouen, F., Halevi, B., & Mukerjee, S. (2016). *Spectroscopic insights into the nature of active sites in iron–nitrogen–carbon electrocatalysts for oxygen reduction in acid*. *Nano Energy*, vol. 29, pp. 65–82. https://doi.org/10.1016/j.nanoen.2016.03.025

Kraytsberg, Ein-Eli, A., Yair. (2014). *Review of Advanced Materials for Proton Exchange Membrane Fuel Cells*. *Energy & Fuels*, vol. 28, no. 12, pp. 7303–7330. https://doi.org/10.1021/ef501977k

Kruusenberg, I., Alexeyeva, N., Tammeveski, K., Kozlova, J., Matisen, L., Sammelselg, V., Solla-Gullón, J., & Feliu, J. M. (2011). *Effect of purification of carbon nanotubes on their electrocatalytic properties for oxygen reduction in acid solution*. *Carbon*, vol. 49, no. 12, pp. 4031–4039. https://doi.org/10.1016/j.carbon.2011.05.048

Lee, B.-N., Kodir, A., Lee, H., Shin, D., & Bae, B. (2021). *Preparation and Characterization of the Polymeric Antioxidant for Improving the Chemical Durability of Polymer Electrolyte Membranes. Transactions of the Korean hydrogen and new energy society*, vol. 32, no. 5, pp. 308–314. https://doi.org/10.7316/KHNES.2021.32.5.308

Li, J., Ghoshal, S., Liang, W., Sougrati, M.-T., Jaouen, F., Halevi, B., McKinney, S., McCool, G., Ma, C., Yuan, X., Ma, Z-F., Mukerjee, S., Jia, Q. (2016). *Structural and mechanistic basis for the high activity of Fe–N–C catalysts toward oxygen reduction*. *Energy &Environmental Science*, vol. 9, no. 7, pp. 2418-2432. https://pubs.rsc.org/en/content/articlelanding/2016/ee/c6ee01160h

Li, J., Alsudairi, A., Ma, Z.-F., Mukerjee, S., & Jia, Q. (2017). *Asymmetric Volcano Trend in Oxygen Reduction Activity of Pt and Non-Pt Catalysts: In Situ Identification of the Site-Blocking Effect*. *Journal of the American Chemical Society* ,vol. 139, no. 4, pp. 1384–1387. https://doi.org/10.1021/jacs.6b11072

Lilloja, J., Kibena-Põldsepp, E., Sarapuu, A., Kikas, A., Kisand, V., Käärik, M., Merisalu, M., Treshchalov, A., Leis, J., Sammelselg, V., Wei, Q., Holdcroft, S., & Tammeveski, K. (2020). *Nitrogen-doped carbide-derived carbon/carbon nanotube composites as cathode catalysts for anion exchange membrane fuel cell application*. *Applied Catalysis B:* vol. 272, pp.3. https://doi.org/10.1016/j.apcatb.2020.119012

Lilloja, J, Kibena-Põldsepp, E., Sarapuu, A., Douglin, ., Käärik, M & Kozlova, J., Kikas, A. ., Paiste, P ., Aruväli, J ., Leis, J ., Sammelselg, V ., Dekel, D & Tammeveski, K. (2021). *Transition Metal and Nitrogen-Doped Carbide-Derived Carbon/Carbon Nanotube Composites as Cathode Catalysts for Anion-Exchange Membrane Fuel Cells*. *Applied Catalysis B: Environmental*, vol. 11. https://pubs.acs.org/doi/10.1021/acscatal.0c03511

Liu, B., & Bard, A. J. (2002). *Scanning Electrochemical Microscopy. 45. Study of the Kinetics of Oxygen Reduction on Platinum with Potential Programming of the Tip*. The Journal of Physical Chemistry B. vol. 106, no. 49, pp. 12801–12806. https://doi.org/10.1021/jp026824f

Liu, Q., Zhang, H., Zhong, H., Zhang, S., & Chen, S. (2012). *N-doped graphene/carbon composite as non-precious metal electrocatalyst for oxygen reduction reaction. The Journal of Physical Chemistry B*, vol. 81, pp. 313–320. https://doi.org/10.1016/j.electacta.2012.07.022

Lopes, T., Kucernak, A., Malko, D., & Ticianelli, E. A. (2016). *Mechanistic Insights into the Oxygen Reduction Reaction on Metal–N–C Electrocatalysts under Fuel Cell Conditions*. *ChemElectroChem*, vol. 3, no. 10, pp. 1580–1590. https://doi.org/10.1002/celc.201600354

Mamtani K., Jain D., Zemlyanov D., Celik G., Luthman J., Renkes G., C. Co A., and Umit S. Ozkan. (2016). *Probing the Oxygen Reduction Reaction Active Sites over Nitrogen-Doped Carbon Nanostructures (CNx) in Acidic Media Using Phosphate Anion*. ACS Catalysis. vol. 6, no. 10, pp. 7249–7259. https://pubs.acs.org/doi/10.1021/acscatal.6b01786

Monteverde Videla, A. H. A., Osmieri, L., & Specchia, S. (2016). Non-noble Metal (NNM) Catalysts for Fuel Cells: Tuning the Activity by a Rational Step-by-Step Single Variable Evolution. In J. H. Zagal & F. Bedioui (Eds.), *Electrochemistry of N4 Macrocyclic Metal Complexes*, pp. 69–101. https://doi.org/10.1007/978-3-319-31172-2_3

Mooste, M., Kibena-Poldsepp, E., Matisen, L., Merisalu, M., Kook, M., Kisand, V., & Vassiljeva, V. (2018). *Oxygen Reduction on Catalysts Prepared by Pyrolysis of Electrospun Styrene-Acrylonitrile Copolymer and Multi-walled Carbon Nanotube Composite Fibres*. *Catalysis Letters*, vol. 148, no. 7, 1815–1827. https://doi.org/10.1007/s10562-018-2392-6

Mtukula, A & Bo, X & Guo, L. (2016). *Highly active non-precious metal electrocatalyst for the hydrogen evolution reaction based on nitrogen-doped graphene supported MoO2/WN/Mo2N*. Journal of Alloys and Compounds. vol. 692, pp. 614-621. https://doi.org/10.1016/j.jallcom.2016.09.079

Nakamura J., Singh, S., Takeyasu, K. (2019). *Active Sites and Mechanism of Oxygen Reduction Reaction Electrocatalysis on Nitrogen-Doped Carbon Materials*. Advanced Materials, vol. 31, no. 13, pp. 1-17. https://doi.org/10.1002/adma.201804297

Oliveira, M.A.C., Pico, P.P.M., Silva Freitas, W., D'Epifanio, A., Mecheri, B. (2020). *Iron-Based Electrocatalysts for Energy Conversion: Effect of Ball Milling on Oxygen Reduction Activity*. Applied Sciences. vol. 10, no. 15, pp. 5278. https://doi.org/10.3390/app10155278

Pasupathi, S., Calderon Gomez, J. C., Su, H., Reddy, H., Bujlo, P., & Sita, C. (2016). Chapter 3, Advances in HT-PEMFC MEAs. In S. Pasupathi, J. C. Calderon Gomez, H. Su, H. Reddy, P. Bujlo, & C. Sita (Eds.), *Recent Advances in High-Temperature PEM Fuel Cells*. pp. 19–31. https://doi.org/10.1016/B978-0-12-809989-6.00003-7

Pérez-Rodríguez, S., Sebastián, D., Alegre, C., Tsoncheva, T., Petrov, N., Paneva, D., & Lázaro, M. J. (2021). *Biomass waste-derived nitrogen and iron co-doped nanoporous carbons as electrocatalysts for the oxygen reduction reaction*. *Electrochimica Acta*, vol. 387, pp. 1-12. https://doi.org/10.1016/j.electacta.2021.138490

Pollet, B.G., Kocha, S.S., Staffell, I. (2019). *Current status of automotive fuel cells for sustainable transport*. Curr. Opin. Electrochem. vol. 16, pp. 90–95. https://doi.org/10.1016/j.coelec.2019.04.021

Ratso, S., Kruusenberg, I., Joost, U., Saar, R., & Tammeveski, K. (2016). *Enhanced oxygen reduction reaction activity of nitrogen-doped graphene/multi-walled carbon nanotube catalysts in alkaline media*. *International Journal of Hydrogen Energy*, vol. 41, no. 47, pp. 22510–22519. https://doi.org/10.1016/j.ijhydene.2016.02.021

Ratso, S, M. Käärik, M. Kook, P. Paiste, V. Kisand, S. Vlassov, J. Leis, K. Tammeveski. (2018). *Iron and nitrogen co-doped carbide-derived carbon and carbon nanotube composite catalysts for oxygen reduction reaction*. Chem- ElectroChem 5 vol. 5, no. 14, pp. 1827–1836. https://doi.org/10.1002/celc.201800132

Ratso, S., N. Ranjbar Sahraie, M.T. Sougrati, M. Käärik, M. Kook, R. Saar, P. Paiste, Q. Jia, J. Leis, S. Mukerjee, F. Jaouen, K. Tammeveski. (2018a). *Synthesis of highly-active Fe-N-C catalysts for PEMFC with carbide-derived carbons*. Journal of Materials Chemistry A vol. 6, no. 30, pp. 14663–14674. https://doi.org/10.1039/C8TA02325E

Ribeiro, B., Botelho, E., Costa, M., & Bandeira, C. (2017 Carbon nanotube buckypaper reinforced polymer composites. Polímeros. vol. 27, no. 3, pp. 1. http://dx.doi.org/10.1590/0104-1428.03916

Rojas-Carbonell, S., Artyushkova, K., Serov, A., Santoro, C., Matanovic, I., & Atanassov, P. (2018). *Effect of pH on the Activity of Platinum Group Metal-Free Catalysts in Oxygen Reduction Reaction*. *ACS Catalysis*, vol. 8, no. 4, pp. 3041–3053. https://doi.org/10.1021/acscatal.7b03991

Ross, P. N., Lipkowski, J., & John Wiley & Sons. (1998). *Electrocatalysis*. *Recent advances in the kinetics of oxygen reduction*. *Electrocatalysis*, pp. 197–242.

Sealy, C. (2008). *The problem with platinum*. *Materials Today*, vol. 11, no. 12, pp. 65–68. https://doi.org/10.1016/S1369-7021(08)70254-2

Sgarbi, R., Kumar, K., Jaouen, F., Zitolo, A., Ticianelli, E., & Maillard, F. (2021). *Oxygen Reduction Reaction Mechanism and Kinetics on M-NxCy and M@N-C Active Sites Present in Model M-N-C Catalysts Under Alkaline and Acidic Conditions*. *Journal of Solid State Electrochemistry*, vol. 25, no. 1, pp. 45–56. https://doi.org/10.1007/s10008-019-04436-w

Shao, M., Chang, Q., Dodelet, J.-P., & Chenitz, R. (2016). *Recent Advances in Electrocatalysts for Oxygen Reduction Reaction*. *Chemical Reviews*, vol. 116, no. 6, pp. 3594–3657. https://doi.org/10.1021/acs.chemrev.5b00462

Shui, J., Chen, C., Grabstanowicz, L., Zhao, D., & Liu, D.-J. (2015). *Highly efficient nonprecious metal catalyst prepared with metal–organic framework in a continuous carbon nanofibrous network. Proceedings of the National Academy of Sciences,* vol. 112, no. 34, pp. 10629-10634

Stauffer E., Dolan J.A., Newman R. (2008). *Chapter 4 - Chemistry and Physics of Fire and Liquid Fuels*. Fire Debris Analysis.pp. 85-129. https://doi.org/10.1016/B978-012663971-1.50008-7

Tellez-Cruz, M. M., Escorihuela, J., Solorza-Feria, O., & Compañ, V. (2021). *Proton Exchange Membrane Fuel Cells (PEMFCs): Advances and Challenges Polymers*. vol. 13, no. 18, pp. 3064. https://doi.org/10.3390/polym13183064

Vikkisk, M., Kruusenberg, I., Joost, U., Shulga, E., & Tammeveski, K. (2013). *Electrocatalysis of oxygen reduction on nitrogen-containing multi-walled carbon nanotube modified glassy carbon electrodes*. *Electrochimica Acta*, vol. 87, pp. 709–716. https://doi.org/10.1016/j.electacta.2012.09.071

Wang, X.-X., Swihart, M.T., Wu, G. (2019). *Achievements, challenges and perspectives on cathode catalysts in proton exchange membrane fuel cells for transportation*. *Nature Catalysis*, vol. 2, no. 7, pp. 578–589. https://doi.org/10.1038/s41929-019-0304-9

Wang, J., Kim, J., Chio, S., Wang, H., & Lim, J. (2020). *A Review of Carbon-Supported Nonprecious Metals as Energy-Related Electrocatalysts.* Small Methods, vol. 4, no. 10, pp. 1-22. https://doi.org/10.1002/smtd.202000621

Wang, J., Kong, H., Zhang, J., Hao, Y., Shao, Z., & Ciucci, F. (2021). *Carbon-based electrocatalysts for sustainable energy applications*. *Progress in Materials Science*, vol. 116, pp. 1-40. https://doi.org/10.1016/j.pmatsci.2020.100717

Wang, Y., Chen, K., Mishler, J., Cho, S. C., & Adroher, X. (2011). *A review of polymer electrolyte membrane fuel cells: Technology, applications, and needs on fundamental research*. *Applied Energy*, vol. 88, pp. 981–1007. https://doi.org/10.1016/j.apenergy.2010.09.030

Warner, J. H., Rümmeli, M. H., Schäffel F., Bachmatiuk A. (2013). *Chapter 4 - Methods for Obtaining Graphene. Journal of Graphene.* pp. 129-228. https://doi.org/10.1016/B978-0-12-394593-8.00004-7

Xu, H., Wang, D., Yang, P., Liu, A., Li, R., Li, Y., Xiao, L., Ren, X., Zhang, J., & An, M. (2020). *Atomically dispersed M–N–C catalysts for the oxygen reduction reaction*. *Journal of Materials Chemistry A* vol. 8, no. 44, pp. 23187–23201. https://doi.org/10.1039/D0TA08732G

Yuan, X-Z., Song, C., Wang, H., Zhang, G. (2010). Electrochemical Impedance Spectroscopy in PEM Fuel Cells. Fundamentals and Applications. no. 1, pp. 1-37. https://doi.org/10.1007/978-1-84882-846-9

Zhan, C., Zhang, Y., Lian, C., Xie, Y., Thompson, M., Kent, P., Cummings, P., Wesolowski, D.J., Jiang, D. (2017). Figure 23. Computational Insights into Materials and Interfaces for Capacitive Energy Storage. Advanced science. vol. 4, no. 7, pp.19. https://doi.org/10.1002/advs.201700059

Zhang, J. (2008). "PEM Fuel Cell Electrocatalysts and Catalyst Layers. Fundamentals and Applications. vol. 53, no. 4, pp. 219–220. https://doi.org/10.1007/978-1-84800-936-3_17

Zhang, S., Zhang, H., Liu, Q., Chen, S. (2013). Fe-N doped carbon nanotube/graphene composite: Facile synthesis and superior electrocatalytic activity. Journal of Materials Chemistry A. vol. 1, pp. 3302–3308. https://doi.org/10.1039/c2ta01351g

Zhang, Y., Huang, L., Jiang, W., Zhang, X., Chen Y., Wei, Z., Wanac, L., and Hu J. (2016). Sodium chloride-assisted green synthesis of a 3D Fe–N–C hybrid as a highly active electrocatalyst for the oxygen reduction reaction. Journal of Materials Chemistry A. vol 1, no. 1, pp. 1-7. https://doi.org/10.1039/C6TA01655C

Zhao, Y., Yang, L., Chen, S., Wang, X., Ma, Y., Wu, Q., Jiang, Y., Qian, W., and Hu, Z. (2013). "Can Boron and Nitrogen Co-doping Improve Oxygen Reduction Reaction Activity of Carbon

Nanotubes?". Journal of the American Chemical Society. vol. 135, no. 4, pp. 1201–1204. https://doi.org/10.1021/ja310566z

Zhong, G., Wang, H., Yu, H., & Feng, P. (2015). Nitrogen doped carbon nanotubes with encapsulated ferric carbide as excellent electrocatalyst for oxygen reduction reaction in acid and alkaline media. Journal of Power Sources. vol. 286, pp. 495-503. https://doi.org/10.1016/j.jpowsour.2015.04.021

Zitolo, A., Goellner, V., Armel, V., Sougrati, M.-T., Mineva, T., Stievano, L., Fonda, E., & Jaouen, F. (2015). Identification of catalytic sites for oxygen reduction in iron- and nitrogen-doped graphene materials. Nature Materials. vol. 14, no. 9, pp. 937–942. https://doi.org/10.1038/nmat4367

Acknowledgement

I would like to take this opportunity to convey to my supervisors MSc Jaana Lilloja, PhD Elo Kibena-Põldsepp and Professor Kaido Tammeveski, my most heartfelt gratitude, for their hard work, patience, and effort in helping me to complete this thesis, providing me knowledge, guidance, and advice throughout this research, it has been a great honour to learn from the best. I am so grateful to have had the opportunity to gain such valuable experience while working under close supervision.

Regarding the researchers who worked on this bachelor's thesis at the Institute of Physics at the University of Tartu, I would like to express my appreciation for all their hard work.

NON-EXCLUSIVE LICENCE TO REPRODUCE THESIS AND MAKE THESIS PUBLIC

I, Oluwaseun Emmanuel Fetuga,

1. herewith grant the University of Tartu a free permit (non-exclusive licence) to

reproduce, for the purpose of preservation, including for adding to the DSpace digital archives until the expiry of the term of copyright,

Transition metal and nitrogen-doped carbon catalysts based on carbide-derived carbon and carbon nanotubes for proton-exchange membrane fuel cell (PEMFC) application,

supervised by MSc Jaana Lilloja, PhD Elo Kibena-Põldsepp and Professor Kaido Tammeveski.

2. I grant the University of Tartu a permit to make the work specified in p. 1 available to the public via the web environment of the University of Tartu, including via the DSpace digital archives, under the Creative Commons licence CC BY NC ND 3.0, which allows, by giving appropriate credit to the author, to reproduce, distribute the work and communicate it to the public, and prohibits the creation of derivative works and any commercial use of the work until the expiry of the term of copyright.

3. I am aware of the fact that the author retains the rights specified in p. 1 and 2.

4. I certify that granting the non-exclusive licence does not infringe other persons' intellectual property rights or rights arising from the personal data protection legislation.

Oluwaseun Emmanuel Fetuga

31/05/2022